port is therefore growing for a new model of area specification in which patterning of the part of the brain responsible for our higher functions is coordinated by the same basic mechanisms and signaling protein families used to generate patterning in other embryonic organs (*3*–*7*).

Our findings further suggest one type of mechanism by which the area map might be altered in evolution. Area maps in different species share topological features, suggesting broad similarities in patterning mechanism, but they also differ in area position, size, and number (*1*). In primate cortex, for example, multiple visual sensory areas appear to have been added in evolution, each characterized by separate retinotopic maps that show abrupt mirror-image reversals at area boundaries. Our observations suggest that the template of a new area could be generated by a local modulation in signaling by a single growth factor.

References and Notes

1. W. J. H. Nauta, M. Feirtag, *Fundamental Neuroanatomy* (Freeman, New York, 1986).
2. P. Rakic, *Science* **241**, 170 (1988).
3. P. Levitt, M. F. Barbe, K. L. Eagleson, in *Annual Review of Neuroscience*, W. M. Cowan, Ed. (Annual Reviews, Palo Alto, CA, 1997), vol. 20, p. 1.
4. J. L. R. Rubenstein *et al.*, *Cereb. Cortex* **9**, 524 (1999).
5. E. M. Miyashita-Lin *et al.*, *Science* **285**, 906 (1999).
6. K. M. Bishop *et al.*, *Science* **288**, 344 (2000).
7. C. W. Ragsdale, E. A. Grove, *Curr. Opin. Neurobiol.* **11**, 50 (2001).
8. P. H. Crossley, G. R. Martin, *Development* **121**, 439 (1995).
9. Y. Furuta *et al.*, *Development* **124**, 2203 (1997).
10. K. Shimamura, J. L. R. Rubenstein, *Development* **124**, 2709 (1997).
11. E. A. Grove *et al.*, *Development* **125**, 2315 (1998).
12. P. H. Crossley *et al.*, *Nature* **380**, 66 (1996).
13. A. Neubuser *et al.*, *Cell* **90**, 247 (1997).
14. W. Ye *et al.*, *Cell* **93**, 755 (1998).
15. H. Shamim *et al.*, *Development* **126**, 945 (1999).
16. A. S. Tucker *et al.*, *Development* **126**, 51 (1999).
17. M. Heikinheimo *et al.*, *Mech. Dev.* **48**, 129 (1994).
18. C. W. Ragsdale *et al.*, unpublished observations.
19. K. Yasuda *et al.*, *Dev. Growth Differ.* **42**, 203 (2000).
20. S. Agarwala *et al.*, *Science* **291**, 2147 (2001).
21. K. J. Huffman *et al.*, *J. Neurosci* **19**, 9939 (1999).
22. Y. Gitton *et al.*, *J. Neurosci.* **19**, 4889 (1999).
23. M. F. Barbe, P. Levitt, *J. Neurosci.* **11**, 519 (1991).
24. K. Mackarehtschian *et al.*, *Cereb. Cortex* **9**, 601 (1999).
25. S. C. Suzuki *et al.*, *Mol. Cell. Neurosci.* **9**, 433 (1997).
26. C. A. MacArthur *et al.*, *Cell Growth Differ.* **6**, 817 (1995).
27. S. M. Lee *et al.*, *Development* **124**, 959 (1997).
28. J. Xu *et al.*, *Development* **127**, 1833 (2000).
29. S. M. Lee *et al.*, *Development* **127**, 457 (2000).
30. A. Chellaiah *et al.*, *J. Biol. Chem.* **274**, 34785 (1999).
31. C. A. MacArthur *et al.*, *Development* **121**, 3603 (1995).
32. T. Fukuchi-Shimogori, E. A. Grove, unpublished observations.
33. T. A. Woolsey, H. Van der Loos, *Brain Res.* **17**, 205 (1970).
34. H. Van der Loos, T. A. Woolsey, *Science* **179**, 395 (1973).
35. K. F. Jensen, H. P. Killackey, *J. Neurosci.* **7**, 3529 (1987).
36. R. T. Ferri, P. Levitt, *Development* **121**, 1151 (1995).
37. J. Galceran *et al.*, *Development* **127**, 469 (2000).
38. Timed-pregnant CD-1 mice were obtained from the University of Chicago Cancer Research Center Transgenic Facility. Noon of the day on which a vaginal plug is seen is termed E0.5. Animal care was according to institutional guidelines.
39. The expression vector backbone was pEF1/Myc-His C (Invitrogen), with gene expression driven from the human elongation factor 1α promoter enhancer. A 2.2-kb fragment between Pvu II sites containing neomycin and SV40 elements was removed to reduce plasmid size, generating pEFX (*20*). Complementary DNAs encoding mouse FGF8 isoform b, mouse WNT3a, human placental alkaline phosphatase (AP), or a truncated, soluble human FGFR3c (sFGFR3) were inserted into pEFX. *sFGFR3* was generated with 5′-GCCATGGGCGCCCCTGCCTGCGCCCTCGC-3′ and 3′-TCGGGGGGGTTCTTTCCGGACCCGAGGATT-5′ polymerase chain reaction primers and encodes the extracellular portion of FGFR3c.
40. Analysis of 295 *AP*-electroporated cortical hemispheres with gene expression, morphological, cell proliferation, or cell death assays indicates that electroporation under our conditions does not itself disrupt neocortical development.
41. G. Minowada *et al.*, *Development* **126**, 4465 (1999).
42. Most electroporated brains required analysis at P0 or P6, several days after transient ectopic gene expression could be directly detected. To determine the frequency of effective gene transfection, several litters were electroporated at E11.5 with *Fgf8* or *AP* plasmids and harvested 48 hours later. Half of the surviving embryos in each litter showed strong transgene expression (31/60). Consistent with this observation, shifts in area domains (Figs. 2 to 4) were seen at P0 or P6 in about one-half of the mice electroporated with *Fgf8* or *sFGFR3* at E11.5 (n = 56/108 with 52 brains showing no shifts). Shifts were invariably consistent, i.e., in the posterior direction for anterior FGF8 overexpression and in the anterior direction for presumed FGF inhibition. No shifts were seen in mice electroporated with the *AP* control plasmid (n = 0/51). Ectopic S1 barrels (Fig. 5) appeared in 10/37 P6 brains after posterior electroporation of *Fgf8*. This lower frequency of effect may be due to the greater difficulty of successful posterior electroporation. Ectopic S1 barrels were not seen after posterior electroporation of AP (n = 0/24).
43. M. T. Wong-Riley, C. Welt, *Proc. Natl. Acad. Sci. U.S.A.* **77**, 2333 (1980).

44. We thank S. Agarwala, S. Assimacopoulos, P. Mason, C. W. Ragsdale, T. Sanders, and C. S. Wellek for discussion and technical help and advice and C. MacArthur, A. McMahon, G. Martin, S. McConnell, M. Donoghue, M. Takeichi, M. J. Hayman, and A. Rattner for cDNAs. Supported by NIH and the March of Dimes Birth Defects Foundation.

10 July 2001; accepted 10 September 2001
Published online 20 September 2001;
10.1126/science.1064252
Include this information when citing this paper.

Universality and Scaling in the Disordering of a Smectic Liquid Crystal

Tommaso Bellini,[1,2] Leo Radzihovsky,[1] John Toner,[3] Noel A. Clark[1]

We present experimental and theoretical studies of the effects of quenched disorder on one-dimensional crystal ordering in three dimensions. This fragile smectic liquid crystal layering, the material with the simplest positional order, is also the most easily deformed periodic structure and is, therefore, profoundly affected by disorder, introduced here by confinement in silica aerogel. Theory and experiment combine to characterize this system to an extraordinary degree, their close accord producing a coherent picture: crystal ordering is lost, giving way to extended short-range correlations that exhibit universal structure and scaling, anomalous layer elasticity, and glassy dynamics.

A major part of condensed matter physics is directed toward understanding the effects of disorder, defects, and impurities, which are responsible for many materials properties and failures. Theoretical models, which systematically introduce disorder into well-understood clean systems, reveal rich and complex phenomena that challenge and broaden our understanding of statistical physics. The effects of disorder can be dramatic, destabilizing phases (*1*–*3*) and producing new ones (*4*–*7*), as well as altering otherwise "universal" behavior near transitions (*8*, *9*). Liquid crystals (LCs), by virtue of their fluidity, their intrinsically soft elasticity, and their experimental accessibility, offer exceptional opportunites for the study of the structural and dynamical effects of quenched disorder, which can be readily introduced, for example, by confinement within appropriate random porous media. Such studies are also of interest in connection with composite electro-optic materials in which randomness is imposed on the LC, for example, by introduction of polymer or nanoparticles (*10*). The starting point for developing a theoretical description of LCs confined in a random environment is to study the effects of weak random point forces and torques on the LC order, an idealized disordering mechanism that affects molecular location and orientation in random ways but occupies as little physical space as possible. This situation can, in fact, be approached in the laboratory by incorporating the LC into the connected void space of an aerogel, a highly

[1]Department of Physics, University of Colorado, Boulder, CO 80309, USA. [2]INFM, Dipartimento di Chimica e Biochimica Medica, Universitá di Milano, Milano, Italy. [3]Department of Physics, Materials Science Institute, and Institute of Theoretical Science, University of Oregon, Eugene, OR 97403, USA.

porous (up to 98% void) fractal-like network of multiply connected filaments of aggregated 3- to 5-nm diameter silica spheres (*11*) to which the molecules stick.

We have investigated the effects of aerogel disordering on the one-dimensional (1D) periodic array of two-dimensional (2D) liquid-like layers of a smectic A (SmA) LC. We studied octyloxycyanobiphenyl (8CB) (*12*) in the vicinity of and below the nematic-SmA (N-SmA) phase transition temperature T_{NA} = 33.5°C, where the layers melt upon heating into a translationally disordered but long-range orientationally ordered nematic phase (Fig. 1) [Web note 1, (*13*)]. Upon approach to the N-SmA transition, bulk 8CB exhibits precursor critical phenomena characteristic of a second order phase change (including growing local smectic domains for $T \rightarrow T_{NA}^{+}$, softening of the layer compression modulus for $T \rightarrow T_{NA}^{-}$, and divergent heat capacity), which have been extensively studied and are understood in many (but not all) respects using modern theories of critical behavior [Web note 1, (*13*) and (*14*)]. Aerogel confinement enables the study of the effects of additional random perturbation, fixed in space and time (quenched disorder), on the smectic layer order (*15*). X-ray diffraction (XRD) (Fig. 1) provides a direct probe of the layer structure in the presence of this disorder (*16*, *17*) and, in combination with calorimetry (*18*, *19*) and static and dynamic light scattering (*19*–*21*), enables a detailed characterization of the smectic ordering within the aerogel matrix. Close quantitative and qualitative accord between experiment and theory (*22*–*26*) leads to considerable insight into the effects of quenched disorder. The experiments show that even very low-density aerogel destroys the 1D crystalline smectic order, consistent with the theoretical prediction that any quenched disorder—no matter how weak—should do so. The observed remnant local layer order persists out to a macroscopic length scale $\xi(T)$, the "x-ray correlation length," which is not equal to any length characteristic of aerogel structure and can be calculated on the basis of a competition between the randomizing effects of the aerogel and the order-seeking smectic elasticity. On the length scale of $\xi(T)$ (Fig. 1C), only elastic layer undulations are generated; i.e., the disordering does not involve topological (dislocation) defects of the layering, which may or may not be produced at longer length scale. The smectic elasticity itself is altered radically, with the shape of the x-ray structure factor providing evidence for predicted anomalous length-scale dependence of the elastic moduli, a result of the disorder-induced layer undulations interacting via smectic elastic nonlinearity. Lastly, the structural correlations of the short-range smectic order exhibit universality and scaling relations; i.e., the host system-specific behavior is lost once the local order becomes extended, as it is in bulk systems near continuous phase transitions. The theory also predicts that, for weak disorder, the topological defects can be expelled by way of a thermodynamically sharp phase transition to produce a topologically and orientationally ordered (but elastically distorted) "smectic Bragg glass" phase. Experimentally, the appearance of activated glass-like dynamics exhibiting divergent logarithmic-in-time slowing with decreasing T (*21*) in combination with the evidence for anomalous elasticity suggest that the smectic Bragg glass is approached at low temperature in the 8CB-aerogel system.

SmA 1D layering is described by the complex order parameter $\psi(\mathbf{r}) \equiv |\psi(\mathbf{r})|\, e^{iq_0 u(\mathbf{r})}$, with $|\psi(\mathbf{r})|$ characterizing the strength of the density modulation and $u(\mathbf{r})$ the smectic layer displacement relative to that of perfect 1D crystalline order of layer periodicity $d = 2\pi/q_0$. As pointed out by deGennes (*27*) this two-component order is analogous to that of superfluids and superconductors. The clean bulk N-SmA transition can be described in two complementary ways, either of which, in principle, can provide a quantitative theory of its thermodynamic singularities [Web note 1, (*13*)]. The Landau-deGennes (LDG) model expands the smectic free energy density in symmetry-allowed powers of ψ and its gradients (*28*), the first three terms to the left describing the bulk N-SmA system and the terms to the right and in curly brackets coupling the random potentials $\mathbf{g}(\mathbf{r})$ and $V(\mathbf{r})$ to $\mathbf{n}(\mathbf{r})$ and $\psi(\mathbf{r})$, respectively, in order to account for the effects of disorder

$$F_{LDG} = F[|\psi|^2] + |\mathbf{c}\cdot(\nabla - iq_0\delta\mathbf{n}(\mathbf{r}))\psi(\mathbf{r})|^2 + F_N[\delta\mathbf{n}(\mathbf{r})] - \{[\mathbf{g}(\mathbf{r})\cdot\mathbf{n}(\mathbf{r})]^2 - \mathrm{Re}[V(\mathbf{r})\psi(\mathbf{r})]\} \quad (1)$$

Here, the minimum of the polynomial $F[|\psi|^2]$ establishes the most probable value of $|\psi|$ (equal to 0 in the N phase and > 0 in the SmA), the second (gradient) term stabilizes the layer thickness to d and the layer orientation to be locally normal to the local average molecular axis orientation, $\mathbf{n}(\mathbf{r})$, and F_N is the energy cost for spatial variation of $\mathbf{n}(\mathbf{r})$, favoring uniform $\mathbf{n}$ (*29*). The complementary elastic (EL) model, which, in the SmA phase below T_{NA}, can be obtained from the LDG at long length scales, expresses the energy density in terms of layer compression $\partial_z u(\mathbf{r})$ and curvature $\nabla_\perp^2 u(\mathbf{r})$ and corresponding compressional (B) and curvature (K) elastic constants (*30*)

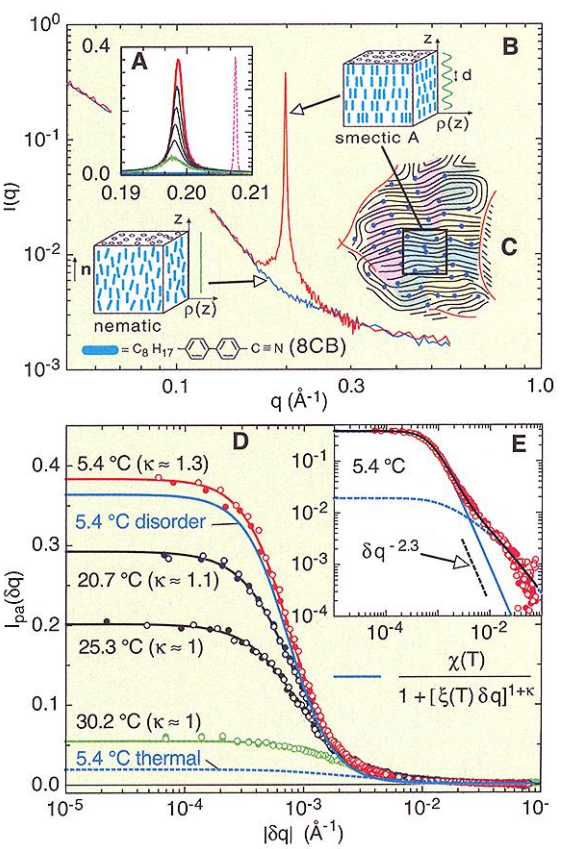

Fig. 1. X-ray structure factor of 8CB in the ϕ = 0.05 aerogel. **(A)** Progressive growth of the smectic peak for 30°C (green curve) > T > 5.4°C (red curve), showing I(q) on a linear scale. Comparison with the much narrower diffractometer resolution (dotted curve) indicates that the smectic correlation length in aerogel is always finite. **(B)** X-ray intensity I(q) showing the 8CB layering peak at wavevector $q_0 \approx q_{bulk} = 2\pi/d = 0.198$ Å^{-1} recorded at T = 5.4°C (red line) on the top of the background scattering from the silica structure recorded at T = 40°C, at the top end of the 8CB nematic range (blue line). **(C)** Pictorial description of a weakly disordered smectic domain with its 1D crystal layers (black lines), free of topological layering defect lines (red dislocation lines), but deformed by pinning sites (blue dots). Background colors highlight regions of correlated order, their size representing ξ. The growth of ξ in the data occurs for ξ much smaller than the typical distance between free dislocations. In the Bragg glass phase, the free dislocations are completely expelled. **(D)** Background-subtracted, resolution-deconvolved peaks $I_{pa}(\delta q)$ plotted versus $|\delta q| = |q - q_o|$. The symmetry, i.e., the overlap of the $\delta q > 0$ (open) and $\delta q < 0$ (closed) points, indicates suppression of the bulk divergence of $\xi_\parallel/\xi_\perp$ (*17*). Fits to $I_d(\delta q) = \chi/[1 + (\xi\delta q)^{1+\kappa(T)}]$ plus a small thermal term are excellent (*40*). **(E)** Fitted $I_{pa}(\delta q)$ at T = 5.4°C showing the disorder compenent (Eq. 4) and thermal component (from powder average of Eq. 3). At low T, the $I_d(\delta q)$ tails fall as $\delta q^{-1+\kappa}$ with $\kappa > 1$, indicative of a crossover to anomalous elasticity.

$$F_{EL} = 1/2\ B[\partial_z u - 1/2(\nabla_\perp u)^2]^2 + K[\nabla_\perp{}^2 u(\mathbf{r})]^2 - 1/2\ \{g_z(\mathbf{r})\mathbf{g}(\mathbf{r})\cdot\nabla_\perp u - \langle\psi\rangle \mathrm{Re}[V(\mathbf{r})e^{2iqou(r)}]\}. \quad (2)$$

The lack of resistance to shear [absence of the $\nabla_\perp u(\mathbf{r})$ term] makes the smectic layer system especially soft and elastically anisotropic (*31*), leading to a variety of exotic elastic effects (*30*), several of which require the nonlinear term (*32*), $-1/2(\nabla_\perp u)^2$, the apparent fractional change in the thickness of the layers when they tilt (*33*). This nonlinearity must be included in a proper description of layer distortions in response to quenched disorder.

The connection between theory and experiment is made by calculating the correlation function and its Fourier transform, the local structure factor $I_{loc}(\delta q)$ with $\delta q = \mathbf{q} - \mathbf{q}_o$, which describes how the local layer order deviates from that of a perfect smectic (*34*). The LDG model with disorder (DLDG) predicts distinct thermal and disorder components of $I_{loc}(\delta\mathbf{q}|\mathbf{n})$

$$I_{loc}(\delta\mathbf{q}|\mathbf{n})_{DLDG} \propto \frac{A_{thermal}}{1 + (\xi_\parallel\delta q_\parallel)^2 + (\xi_\perp\delta q_\perp)^2} + \frac{A_{disorder}}{[1 + (\xi_\parallel\delta q_\parallel)^2 + (\xi_\perp\delta q_\perp)^2]^2} \quad (3)$$

where the correlation lengths $\xi_\parallel$ and $\xi_\perp$ characterize the extent of local order parallel and normal to the local nematic orientation $\mathbf{n}$ (*35*). In the bulk clean nematic ($A_{disorder} = 0$), experiment finds (*14*) and LDG (*36*, *37*) or EL (*38*, *39*) theory predicts that $\xi_{\parallel N}(T) \neq \xi_{\perp N}(T)$ ($c_\parallel \neq c_\perp$ in Eq. 1) and that they diverge at different rates as $T \rightarrow T_{NA}$. This divergent bulk anisotropy ($\xi_{\parallel N}(T)/\xi_{\perp N}(T) \rightarrow \infty$) is unique to the N-SmA transition among the analogous two-component order parameter systems, arising from the coupling of $\mathbf{n}(\mathbf{r})$ to the layer ordering (*14*). The $\mathbf{g}$ and V terms, which couple disorder directly to $\mathbf{n}$ and ψ of the smectic, are forbidden by gauge symmetry in superconductors and superfluids, enabling, for example, the normal-superfluid transition in ^{4}He to survive aerogel disordering (*8*). Because $\mathbf{g}$ and V are predicted to dramatically enhance the effects of disorder in smectics (*24*), it is of interest to see how the deGennes analogy between smectics and quantum systems fares in the presence of quenched disorder.

8CB in aerogel. The x-ray scattering structure factor I(q) of 8CB (*12*) in the least dense aerogel studied is shown (Fig. 1). Even in the aerogel of lowest solid fraction at the lowest temperature studied, where the effects of the aerogel on smectic order should be the weakest, we find that the width Δq of the smectic layering peak is finite and measurable (*17*) (Fig. 1A), in contrast to the effectively resolution-limited Bragg reflection of bulk 8CB (*15*). Thus, the bulk smectic quasi–long range order is suppressed at lengths greater than $\xi \sim \Delta q^{-1}$. Quantitatively, the peak due to the layering is obtained by removing from I(q) the effects of the diffractometer resolution and the background scattering (*40*). The resulting structure factor data, $I_{pa}(\delta q = q - q_o, T)$ must be compared with the orientational (powder) average of $I_{loc}(\delta\mathbf{q}|\mathbf{n})$ the averaging over $\mathbf{n}$ accounting for the overall isotropy of the aerogel system. Figure 1, D and E, shows that the disorder term is the dominant feature of $I_{pa}(\delta q)$ for $T < T_{NA}$, but that the disorder and the thermal components are identifiable; the thermal part appears in the tails because of its weaker decay in comparison to δq, as in Eq. 3. The disorder component of $I_{pa}(\delta q)$ was fit to the simple theoretically motivated function

$$I_d(\delta q, T) = \frac{\chi(T)}{1 + [\xi(T)\delta q]^{1+\kappa(T)}} \quad (4)$$

which provides an excellent description of $I_{pa}(\delta q, T)$ and yields $\kappa \approx 1$ throughout most of the (ϕ, T) range. Such a result supports the DLDG model, because Eq. 4 with $\kappa = 1$ is the powder average of the disorder term of the DLDG I_{loc} of Eq. 3 (*41*). However, the exponent κ is found to systematically increase to $\kappa \approx 1.3$ for low ϕ and low T (Fig. 1, D and E, and Fig. 4B). Calculation of the tails of $I_{loc}(\delta\mathbf{q})$ and $I_d(\delta q)$ using the disordered EL (DEL) model (*26*) shows that this increase of κ provides evidence for a crossover to "anomalous elasticity."

The x-ray susceptibility $\chi(T)$ and correlation length $\xi(T)$ extracted from the fits (Fig. 2) are quite remarkable. The disordering is strong enough to make $\xi(T)$ small compared with the bulk nematic correlation length $\xi_{\parallel N}(T)$ for $T > T_{NA}$ and to exhibit no sign of the bulk divergence of $\xi_{\parallel N}(T)$ as $T \rightarrow T_{NA}$. Nevertheless, the smectic layering is able to expel disorder, albeit only gradually, over a broad range of $T < T_{NA}$. Thus, ξ is set neither by the bulk behavior nor by some intrinsic pore size of the aerogel, but rather by the competition between the disordering influence of the aerogel and the smectic elasticity, whose rigidity increases with decreasing T (*42*, *43*). The amplitude $\chi(T)$, shown in Fig. 2B for three aerogels, is proportional to the susceptibility of the system to a periodic perturbation at wavevector q_0, and, like $\xi(T)$, continues growing for T well below T_{NA}. Plots of $\chi(T)$ versus $\xi(T)$ (Fig. 2C) show that the scaling relation $\chi \propto \xi^2$, a general feature of fluctuations near second order transitions and approximately satisfied in bulk 8CB for $T > T_{NA}$ (*44*), also holds for smectic ordering in the aerogel over much of the ϕ,T range. This, along with the finiteness of $\xi(T)$, indicates that the aerogel-LC system is behaving as if the smectic phase is being approached but never reached. The rounding of the peaks of $\Delta C_p(T)$, the heat capacity anomaly associated with the smectic ordering (*18*) (Fig. 3), and their shift to lower T are also indicative of the elimination of the N-SmA phase transition. However, the basic peak structure indicates the survival of the two regimes of ordering characteristic of the bulk. For $T > T_{peak}$, ΔC_p increases with decreasing T, a result of the increased noise in the enthalpy coming from the increased fluctuation amplitude at small q that accompanies growth in correlation. For $T < T_{peak}$ ΔC_p decreases with decreasing T, indicating progressive quenching of the fluctuations about the local smectic order. In the bulk, the phase transition singularity makes the distinction between these two regimes sharp, whereas in the aerogel it appears as a continuous crossover (at the maximum in ΔC_p). The characteristics of this change from growth of correlation (solid circles in Fig. 3) to the quenching of fluctuations (open circles in

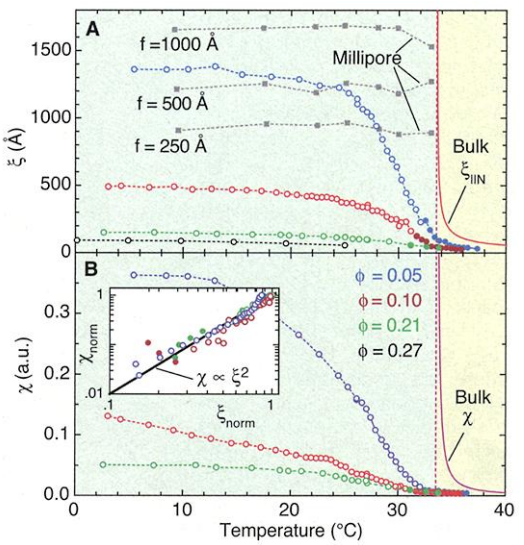

Fig. 2. Temperature dependence of the smectic correlation length ξ (T) and susceptibility χ(T) of 8CB in aerogels. ξ(T) (**A**) and χ(T) (**B**) increase only gradually with decreasing T, with ξ(T) requiring ~10°C below the bulk T_{NA} to begin to saturate a low T value, which depends on silica volume fraction ϕ (*17*). This contrasts with the bulk behavior (solid lines) and with the correlation lengths measured in Millipore (gray squares) which abruptly saturate at $T \cong T_{NA}$ at values governed by the pore size, f (*42*). The inset plots ξ(T) versus χ(T), where these quantities are scaled to overlap for 25°C < T < 33°C, showing that in this regime where the disordered LDG description should apply and $\kappa \approx 1$, the predicted $\chi \propto \xi^2$ scaling relation is obeyed. This scaling breaks down at lower T in the lowest density aerogels, where $\kappa > 1$ due to anomalous elasticity. Solid circles are in the growth of correlation regime and the open circles in the quenching of fluctuations regime (see Fig. 3).

Fig. 3) can be understood by noting that the rounding and shift of ΔC_p is reminiscent of the critical behavior of finite-size systems (*45*, *46*), wherein the ΔC_p peak occurs at the $T_c(L)$ where the bulk correlation length of fluctuations about the ordered state ($\xi_{\|S}(T)$ in the SmA) (Fig. 3) becomes comparable to the system size L, which is also the maximum correlation dimension (achieved when T crosses T_c). For the aerogel-confined LC, we find that it is the continuously growing $\xi(T, \phi)$, the correlation range actually achieved for $T < T_{NA}$, that acts as the effective finite-size cutoff, playing the role of L. This condition is expressed by the geometrical constructions in Fig. 3: The position T_{peak} of the ΔC_p peak is predicted by the orange line construction to occur when $\xi(T_{peak}, \phi) = \xi_{\|S}(T_{peak})$; the peak value of ΔC_p, predicted by the gray line construction, is the value the bulk ΔC_p would have achieved due to order fluctuations in the bulk nematic when $\xi_{\|N} = \xi(T_{peak}, \phi)$. The ($\Delta C_p$, T) coordinates of the peak obtained in this way (colored diamonds) agree well with those of the ΔC_p data in the different aerogels. Thus, although the bulk second order N-SmA transition is suppressed, the length scale $\xi(T)$ of the remnant local order is sufficiently large that the principal characteristics of $\Delta C_p(T)$ can be understood on the basis of the generalized finite size scaling behavior of a bulk clean system cutoff by $\xi(T)$ (*47*).

Theory and Interpretation. The orientational and positional pinning of smectic layers produced by aerogel confinement is introduced to the theoretical description of the N-SmA system by the functions $\mathbf{g}(\mathbf{r})$, representing the random torque on the local average molecular orientation $\mathbf{n}(\mathbf{r})$, and $V(\mathbf{r})$, the local random force on the smectic layers (Eqs. 1 and 2). Note that $V(\mathbf{r})$ is a periodic function of the layer displacement $u(\mathbf{r})$, with a period equal to the smectic layer spacing, reflecting the discreteness of the layers and the fact that the pinning cannot be selective as to which specific layer to pin; i.e., a randomly pinned smectic is invariant under relabeling of the layers. This periodicity has important consequences at long length scales, where, because of the growth of the fluctuations of $u(\mathbf{r})$ induced by the random torque $g(\mathbf{r})$, the $V(\mathbf{r})$ term effectively averages to zero, becoming subdominant to $g(\mathbf{r})$ for static correlations [although remaining dominant for dynamics (*26*)]. Because the pinning of the LC to the aerogel varies on a sub-nanometer scale, the disordering potentials $\mathbf{g}(\mathbf{r})$ and $V(\mathbf{r})$ are random functions with only short-ranged correlations, despite any long scale (e.g., fractal) correlations in aerogel density. In this case $\mathbf{g}(\mathbf{r})$ and $V(\mathbf{r})$ are the potentials necessary and sufficient to account for all long length scale manifestations of disorder. We have recently made considerable progress in developing theoretical tools that enable detailed understanding of smectic ordering in random structures (*22*–*25*), and we have used these tools to analyze the long-scale properties of both the DLDG (*25*) and DEL models (*22*–*24*), finding substantial agreement with experiment (*48*–*51*).

A key prediction of the theory, emerging from both the DLDG and the DEL descriptions is that the deGennes' analogy does not survive quenched disorder (*52*). Specifically, the introduction of $\mathbf{g}(\mathbf{r})$, which is forbidden at long scale by gauge symmetry in the in quantum systems, destroys the layering of the bulk clean smectic. The analysis of the LDG equation with disorder incorporated as a perturbation shows that any amount of disorder, however weak, effectively drives $T_{NA} \rightarrow 0$ for spatial dimensions $D < 4$ (*23*, *53*). The correct and detailed interpretation of this result emerges from the DEL description (rigorous for weak disorder), which predicts that 3D smectics are unstable in the presence of any—even infinitesimal—amount of disorder. Quantitative contact with the x-ray measurements near T_{NA} is made by calculating $I_{loc}(\delta\mathbf{q})$ with the use of a Gaussian approximation to the DLDG with, as input, correlation lengths that are finite for all T, derived from an independent calculation and perturbative in the disorder variances Δ_V, and Δ_g of $V(\mathbf{r})$ and $\mathbf{g}(\mathbf{r})$, respectively (*25*). The result is a simple, random-field XY model (*50*), with all the effects of $\mathbf{g}(\mathbf{r})$ and some of the effects of $V(\mathbf{r})$ incorporated into the finite correlation lengths, which leads to $I_{loc}(\delta\mathbf{q})_{DLDG}$ of Eq. 3 with renormalized $A_{thermal}(T, \Delta_V)$, $A_{disorder}(T, \Delta_V)$, and $\xi_{\|,\perp}(T, \Delta_V)$ that depend only on Δ_V (*25*). As Δ_V increases, the disorder (Δ_V) term comes to dominate the T dependence of $I_{loc}(\delta\mathbf{q},T)$ for $T < T_{NA}$, giving the powder average $I_d(\delta q,T)$ of Eq. 4 with $\kappa = 1$ in agreement with the symmetric line shapes observed at higher T and describing all of its T and ϕ dependence very well, e.g., $\xi(T, \phi)$ as shown in Fig. 3A (*25*, *54*).

The DEL energy of Eq. 2 is a complete first-principles description of the smectic in weakly disordering random media. The allowed quenched disorder explicitly breaks the translational and orientational symmetry of the ordered state, introducing energy terms that couple directly to smectic layer positions and orientations, which are characterized by scalar displacement u and ∇u, respectively. As for other condensed phase systems with spontaneous translational order (*55*), the resulting elastic deformation can involve both continuous displacement (akin to thermally driven lattice vibrations) as well as singular jumps arising from topological defects (dislocations). It is a key challenge in the study of such disordered elastic media to determine the role of each mechanism. Detailed analysis of the DEL model of Eq. 2 in the limit of weak disorder predicts that the loss of layer coherence takes place at the length scale $\xi(T)$ at which the pinning disorder energy begins to dominate over the smectic elastic energy, but does so without creation of dislocations, i.e., without breaks in the layers (Fig. 1C) (*22*). Free dislocations, if present, have much larger separations (Fig. 1C) and may not appear at all if the disorder is sufficiently weak.

Because of the soft-layer undulation degrees of freedom of the smectic (expressed by the absence of $\nabla_\perp u$ linear elasticity), the lowest order nonlinear elastic term in the DEL model of Eq. 2 qualitatively modifies the long scale elastic properties of bulk smectic liquid crystals (*32*). Although the resulting effects are not detectable in bulk static experiments, the impor-

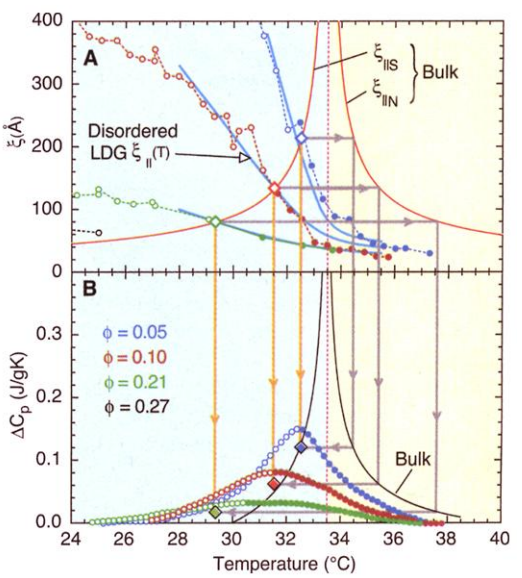

Fig. 3. Generalized finite-size scaling in disordered smectic. (**A**) Correlation length $\xi(T)$ and (**B**) specific heat $\Delta C_p(T)$ (*18*) measured in the aerogels for $T \sim T_{NA}$, along with bulk correlation lengths (red lines) and bulk $\Delta C_p(T)$ (black lines). ΔC_p data from the $\phi = 0.27$ aerogel are not reported because the peak is depressed to the point of being undetectable. For $T > T_{peak}$ (solid circles), the system is thermally nematic-like, with ψ fluctuating around a 0 average, whereas for $T < T_{peak}$ (open circles), the dominant behavior is the smectic-like quenching of fluctuations about a nonzero local ψ. An argument in the spirit of finite-size scaling gives reasonable estimates of T_{peak} and $\Delta C_{p,peak}$ (solid diamonds): the position T_{peak} is the crossover T where $\xi_{\|S}(T) = \xi(T)$ (open diamond and orange line construction); the peak value of ΔC_p is the bulk ΔC_p for a bulk nematic correlation length equal to the aerogel correlation length when the crossover $\xi = \xi_{\|S}$ occurs (gray line construction) (*47*). The light blue curves indicate the disordered LDG prediction (*25*), which gives an excellent fit to the $\xi(T)$ data set for $T \cong T_{NA}$ by varying only the disorder variance Δ_V. The latter is found to scale with the aerogel solid fraction as $\Delta_V \sim \phi^{1.6}$

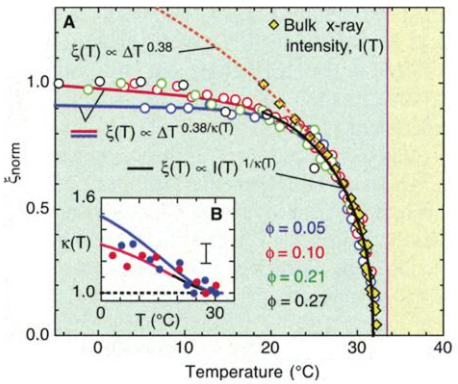

Fig. 4. Elastic scaling in weak disorder. **(A)** ξ(T) measured for the different aerogels (open circles) and normalized to overlap for 25°C < T < 33°C collapse into a single curve that matches the B(T) ∝ I(T) ∝ $t^{0.38}$ growth of the smectic layer compressional elastic constant B(T), obtained from I(T), the measured integrated bulk x-ray intensity (*v*), available above freezing (dashed line). This match indicates that κ = 1 in this T range, consistent with κ obtained from the x-ray lineshapes in **(B)**. The black lines in (A) and (B) are ξ(T) ~ $I(T)^{1/\kappa(T)}$ and the κ(T) necessary to fit the aerogel ξ(T) for 19 °C < T < 25°C, respectively. The red and blue lines are similarly obtained for ϕ = 0.10 and 0.05, respectively, by assuming that the B(T) ∝ $t^{0.38}$ dependence persists for T < 19°C, where bulk I(T) data are not available. These κ(T) are qualitatively consistent with those in (B) obtained from the line shapes.

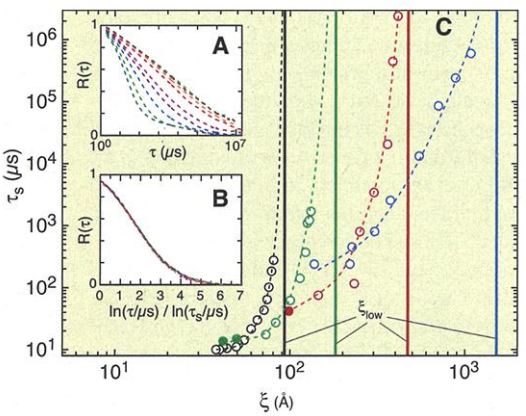

Fig. 5. Smectic slowing down. **(A)** R(τ), autocorrelation functions of light scattered by orientation fluctuations of 8CB in the 0.36 g/cm^3 aerogel at different T, ranging from T = 31.0°C (fastest decay) to T = 18.2°C (slowest decay). The R(τ) exhibit a slow mode not observed on bulk single domain samples. This mode, which is controlled by dislocation motion, requires many decades in time to relax, and exhibits dramatic slowing down with decreasing T as evidenced by the increase in scaling time for relaxation τ_s. **(B)** Scaling the lnτ axis by lnτ_s collapses the R(τ) onto a single curve. Such a remarkable collapse is observed in the quenching of fluctuations regime (open circles) but not in the growth of correlation regime (solid circles). **(C)** The slowing diverges as ξ approaches its low-temperature values with decreasing T. Because of the light is multiply scattered R(τ) is basically independent of scattering angle (*21*).

tance of this nonlinearity is significantly and qualitatively amplified in randomly confined smectics because fluctuations caused by the disorder-induced smectic roughness are even larger and interact with each other through the nonlinear elastic term. Detailed renormalization group calculations show that, at sufficiently long length scales, this leads to a bizarre "anomalous elasticity" (AE), wherein the elastic "constants" B and K become functions of wavevector q, with B(q) → 0 and K(q) diverging as q → 0 (B(q) ~ q^{η_B}, K(q) ~ $q^{-\eta_K}$ (*22*), where η_B and $\eta_K > 0$ are universal exponents, predicted to be independent of T, ϕ, and the structural details of the disordering medium. Analysis of the short length scale behavior of $\langle u(r)^2 \rangle$ shows that, after powder averaging, $I_d(\delta q) \propto \delta q^{-(\kappa+1)}$ in the tails of the peak (*26*), where $\kappa \equiv [2/(\eta_B + \eta_K) - 1/2]^{-1}$ and κ ≠ 1 indicates the presence of AE (*56*). ξ(T) is predicted to grow as ξ(T) ~ $\Delta_g^{-1} K^{2-1/\kappa} B(T)^{1/\kappa}$ (*22*, *57*), a relation that expresses explicitly the aforementioned competition between disorder and elasticity.

The x-ray lineshapes $I_{pa}(\delta q)$ and the growth of ξ(T) show independent evidence for AE at lower T (< 25°C), as indicated in Fig. 4. For higher T (> 25°C) the growth of ξ(T) in the different aerogels can be simply scaled to mutually overlap, confirming the basic scaling prediction of $\tilde{\xi}$. Furthermore, the overlapped ξ(T) grow as B(T) (as determined from the bulk powder-averaged integrated x-ray peak intensity I(T) ~ $t^{0.38} \propto \langle |\psi(\mathbf{r})|^2 \rangle \propto B(T)$ (*58*–*60*). This growth is consistent with ξ(T) ~ $B(T)^{1/\kappa}$ with κ ≈ 1. For T > 25°C in all of the aerogels, $I_{pa}(\delta q)$ is found to be Lorentzian (κ ≈ 1). However for T < 25°C, the aerogel ξ(T) begins to systematically fall below the bulk B(T) (available for T > 19°C, where bulk 8CB freezes), indicative of the effects of AE. The $I_{pa}(\delta q)$ fits yield κ > 1 for the lowest density aerogels (Fig. 4B). Allowing a T-dependent κ in ξ(T) ~ $B(T)^{1/\kappa(T)}$ to fit the aerogel ξ(T) from the bulk I(T) data, yields the solid black curves in Fig. 4, A and B. These and the red and blue curves, obtained if the bulk B(T) ~ $t^{0.38}$ power law behavior observed for T > 19°C (dotted curve) is assumed to apply over the entire T range, also show an increase in κ(T) (Fig. 4B) similar to that found from the $I_{pa}(\delta q)$ (*61*). The theory interprets this apparent T dependence of κ as a crossover, occurring as ξ(T) increases through the length scale at which AE becomes important, that fits smoothly interpolating κ from the fixed exponent κ = 1 of conventional elasticity to a fixed κ for AE. Presumably, the lowest T value κ ≅ 1.3 (implying $\eta_B + \eta_K \cong 1.55$) is the closest to the universal value for smectic disorder in 3D, which can only be roughly estimated from the theory (*62*). Despite the subtleties of the crossover behavior, the consistency of the values of κ obtained independently from the line shapes and from the growth of ξ(T) indicates the validity of the theory, and, given the κ obtained, the potential for an unknown "Smectic Bragg Glass (SmBG)" phase.

Glassy dynamics. In the bulk smectic, the dynamics of the quasi–long range ordered layering can be described in terms of phononlike fluctuations that become faster as T is lowered and the local smectic rigidity B(T) increases. Evidence for this dynamical behavior has been obtained from the Quasi Elastic Light Scattering (QELS), produced by the director reorientation accompanying layer tilt fluctuations (*63*, *64*). As shown in Fig. 5, QELS is also an effective way of probing smectic layer dynamics in the aerogel (*65*), revealing a new mode for T < T_{NA}, unknown in the bulk and unambiguously assignable to layer fluctuations, that exhibits radical slowing as T is lowered (*21*). QELS time correlation functions R(τ) exhibit a slow decay over many decades in τ, describable as a universal (approximately Gaussian) function of ln(τ)/ln(τ_s), where τ_s is an appropriate T-, ϕ-dependent stretching time scale that appears to diverge in each aerogel as ξ(T) begins to saturate at low T. Such scalable "stretched" decay of correlations and divergent scaling times indicate that the 1D layering system is becoming glasslike with decreasing T (*2*, *66*).

A specific realization of such a scenario is the divergence predicted in the weak disorder limit as a precursor to a continuous transition from the nematic to the thermodynamically distinct SmBG (*22*). On the high-T side of this transition, the liquid crystal is locally topologically ordered (dislocation free) as a smectic, with ξ(T) established by continuous elastic layer undulations, but at long length scales is topologically disordered, with free topological layering defects (unbound dislocations, red lines) proliferating (*67*). The SmBG is similarly characterized by elastically disordered layers, but has only bound dislocations on long length scales (*68*–*74*). Here, the divergent smectic glass correlation length and the associated slowing arise from the increasing distance between the unbound dislocations, as these defects are expelled when the SmBG-N transition temperature is approached from above. The Gaussian in log τ dynamic correlations that we observe, then, are a natural property associated with activation of this topologically correlated state over energy barriers that diverge with a power of the size of the active regions (*75*–*77*).

References and Notes

1. D. S. Fisher *et al.*, *Phys. Today* **December**, 56 (1988).
2. K. Binder, A. P. Young, *Rev. Mod. Phys.* **58**, 801 (1986).
3. B. J. Frisken *et al.*, *Phys. Rev. E* **51**, 5922 (1995).
4. J. L. Cardy, S. Ostlund, *Phys. Rev. B* **25**, 6899 (1982).
5. J. Toner, D. P. DiVicenzo, *Phys. Rev. B* **41**, 632 (1990).
6. M. P. A. Fisher, *Phys. Rev. Lett.* **62**, 1415 (1989).
7. D. S. Fisher *et al.*, *Phys. Rev. B*, **43**, 130 (1991).
8. M. Chan *et al.*, *Phys. Today* **August**, 30 (1996).
9. K. Moon, S. M. Girvin, *Phys. Rev. Lett.* **75**, 1328 (1995).
10. *Liquid Crystals in Complex Geometries*, G. P. Crawford, S. Zumer, Eds. (Taylor and Francis, London 1996).
11. Aerogels can be visualized as nanoscale silica tumbleweed piles, made in solution by aggregation of 3- to 5-nm-diameter silica particles into fractal clusters and gelation of these clusters, forming a network stabilized by covalent chemical bonds, from which the solvent is then removed. The concentration of the precursor solution and the drying conditions can be varied to produce samples with different mass densities: ρ = 0.08, 0.17, 0.36, and 0.60 g/cm^3 for the present experiments. The silica volume fraction ϕ within these aerogels is small: ϕ = 0.05, 0.10, 0.21, and 0.27, respectively. The internal aerogel structure is characterized by the average lengths of uninterrupted solid and pore regions along a line, respectively; $\langle s \rangle$ is a measure of the filament size, nearly independent of ϕ [$\langle s \rangle$ = 46 ± 4 Å], and $\langle p \rangle$ is a measure of the typical cavity dimension, which decreases with increasing ϕ [$\langle p \rangle$ = 700 Å, 430 Å, 180 Å and 120 Å]. See also (*17*).
12. The neat compound 8CB exhibits isotropic (I), nematic (N), smectic A (SmA), and crystal (X) phases in the bulk as follows: {I (T_{IN} = 40.5°C) N (T_{NA} = 33.5 °C) SmA (T_{AX} = 19°C) X}.
13. Web figs. 1 through 4 and notes 1 through 11 are available at *Science* Online at www.sciencemag.org/cgi/content/full/294/5544/1074/DC1.
14. C. W. Garland, G. Nounesis, *Phys. Rev. E* **49**, 2964 (1995).
15. See note 2, (*13*).
16. N. A. Clark *et al.*, *Phys. Rev. Lett.* **71**, 3505 (1993).
17. A. G. Rappaport *et al.*, chap. 20 of (*10*).
18. L. Wu *et al.*, *Phys. Rev. E* **51**, 2157 (1995).
19. T. Bellini *et al.*, *Phys. Rev. Lett.* **69**, 788 (1992).
20. T. Bellini *et al.*, *Phys. Rev. Lett.* **74**, 2740 (1995).
21. T. Bellini, N. A. Clark, chap. 19 of (*10*).
22. L. Radzihovsky, J. Toner, *Phys. Rev. Lett.* **79**, 4214 (1997).
23. ———, *Phys. Rev. Lett.* **78**, 4414 (1997).
24. ———, *Phys. Rev. B* **60**, 206 (1999).
25. B. Ward, Ph.D. Thesis, University of Colorado (1999); L. Radzihovsky, B. Ward, unpublished theory.
26. L. Radzihovsky, J. Toner, unpublished theory.
27. P. G. deGennes, *Solid State Commun.* **10**, 753 (1972).
28. The LDG equation is the analog for the SmA system of the Landau-Ginzburg equation, describing the normal metal to superconductor transition in which Ψ gives the amplitude and the phase of the electron Cooper pair condensate wavefunction. Smectics, superconductors, superfluids, and other systems that have two-component order parameters exhibit a variety of common phenomenology but, as we show, can differ drastically when subjected to quenched disorder.
29. See note 3, (*13*).
30. P. G. deGennes, J. Prost, *The Physics of Liquid Crystals* (Oxford Univ. Press London, 1993), chaps 7 and 10.
31. The leading bulk terms in the "elastic" description are quadratic in the spatial derivatives of layer displacement, a consequence of the spontaneous translational symmetry breaking of the clean smectic. See note 4, (*13*).
32. G. Grinstein, R. A. Pelkovitz, *Phys. Rev. Lett.* **47**, 856 (1981).
33. N. A. Clark, R. B. Meyer, *Appl. Phys. Lett.* **22**, 493 (1973).
34. See note 5, (*13*).
35. The correlation length $\xi_{\|}(T)$ is the same for the thermal and the disorder terms, as it is for $\xi_{\perp}(T)$.
36. T. C. Lubensky, J.-H. Chen, *Phys. Rev. A* **17**, 366 (1978).
37. B. Patton, B. Anderek, *Phys. Rev. Lett.* **69**, 1556 (1992).
38. D. R. Nelson, J. Toner, *Phys. Rev. B* **24**, 363 (1981).
39. J. Toner, *Phys. Rev. B* **24**, 462 (1982).
40. See note 6, (*13*).
41. The symmetry of the $I_{pa}(\delta q)$ peaks (Fig. 1D) indicates that the divergent bulk anisotropy of $\xi_{\|}(T)/\xi_{\perp}(T)$ is suppressed in the aerogel, placing the limit $R(T) \equiv \xi_{\|}(T)/\xi_{\perp}(T) < 3$ (*17*). In this case, $\xi(T)$ fitted in Eq. 4 should be compared with $\xi_{\|}(T)$ in Eq. 3 from the theory. For $\xi_{\|}(T)$ sufficiently large and $\xi_{\|}(T)/\xi_{\perp}(T)$ sufficiently small the (Lorentzian)^2 disorder term of Eq. 3 powder-averages to Eq. 4 with κ = 1.
42. It is useful to compare this 8CB-aerogel behavior with that of other porous hosts. Correlation lengths $\xi(T)$ for 8CB in Millipore porous cellulose is presented with the aerogel data in Fig. 2A. See note 7, (*13*). Results of a detailed study of the ordering of 8CB in the presence of dispersed silica nanoparticles (aerosil) are reported in (*43*). In aerosil, the disordering per unit of silica concentration is less than that in aerogel, suggestive of less disperse organization of the silica particles and/or annealing, which is rearrangement of the disorder in response to smectic ordering.
43. S. Park *et al.*, in preparation.
44. In the bulk, the nematic power law divergences of $\chi(T)$ and $\xi(T)$ exhibit the scaling property $\chi(T) \propto \xi(T)^{\gamma/\nu_{\|}}$, where $\gamma/\nu_{\|}$ = 1.88 [See note 1, (*13*)]. Because the short-range correlations in the aerogel appear to be more isotropic than those of the bulk, we might expect γ/ν in the aerogel to approximate $\gamma/\nu \sim 1.97$, the value of the isotropic 3D XY model. This expectation is borne out by the disordered LDG model.
45. M. E. Fisher, A. E. Ferdinand, *Phys. Rev. Lett.* **19**, 169 (1967).
46. M. E. Fisher, M. N. Barber, *Phys. Rev. Lett.* **28**, 1516 (1972).
47. In a system of finite size L, the scaling relations for the shift in peak position $\Delta T_{peak}(L) \sim L^{-1/\nu}$ and peak heat capacity $\Delta C_{p,peak} \sim L^{\alpha/\nu}$ yield $\Delta C_{p,peak} \sim \Delta T_{peak}^{-\alpha}$ for the trajectory of the maxima of the shifted and rounded heat capacity peaks on the $T < T_{NA}$ side of bulk $\Delta C_p(T)$. This behavior is manifested in the aerogel in Fig. 3.
48. Because of the simultaneous presence of the "gauge" field $\mathbf{n}(\mathbf{r})$ and random field disorder, the treatment of the disordered LDG (DLDG) model is considerably more involved than the mathematically related problems of disordered charge density waves, superconductors, superfluids, and magnets, which have received so much attention in the recent years (*1*). Likewise, because of the simultaneous presence of the elastic and topological defect nonlinearities together with the two types of relevant disorder [$\mathbf{g}(\mathbf{r})$ and $V(\mathbf{r})$], the analysis of the disordered EL (DEL) model is considerably more complicated than the treatment of its mathematically related cousin, the random-field XY-model (*49*–*51*).
49. Y. Imry, S. K. Ma, *Phys. Rev. Lett.* **37**, 1364(1976).
50. G. Grinstein, *Phys. Rev. Lett.* **37**, 944 (1976).
51. D. S. Fisher, *Phys. Rev. B* **31**, 7233 (1985).
52. See note 8, (*13*).
53. For a hypothetical 1D ordered smectic "living" in a high-dimensional space (D > 5), the SmA (quasi) long-range order would be preserved in low-density aerogels (*22*).
54. See note 9, (*13*).
55. See note 4, (*13*).
56. This result holds for $\lambda^2 = K/B \gg d^2$, satisfied in 8CB for $T < T_{NA} - 0.1°C$ ($\lambda^2/d^2 > 20$ for $T < 30°C$). In the opposite limit, it is approached as $T \rightarrow T_{NA}$, $\kappa \rightarrow 1$ (*24*).
57. The Boltzmann energy k_BT does not explicitly appear in $\xi(T)$ because the roughness of the smectic layers is dominated by the quenched disorder and not thermal fluctuations, with the result that the T dependence of $\xi(T)$ is controlled by that of the bulk B(T), because the elastic constant K and the variances of the quenched disorder Δ_g are only weakly dependent on T.
58. The bulk SmA B(T) can be obtained to within a multiplicative constant from the integrated intensity of the bulk powder diffraction quasi-Bragg peak $I(T) \propto \langle |\psi(\mathbf{r})|^2 \rangle \propto B(T)$, assuming the mean field picture to apply in the SmA for T > 19°C, where bulk 8CB freezes. The result is $B(T) \sim |\Delta T|^{0.38}$ for 33°C > T > 19°C (*17*). B(T) can also be obtained from measurement of "second sound" layer compression resonances (*59*), which gives $B(T) \sim |\Delta T|^{0.40}$ for 33.5 > T > 31.5°C, essentially identical B(T) behavior.
59. M. Benzekri *et al.*, *Phys. Rev. B* **41**, 9032 (1990)
60. Although the $\xi(T)$ data in the different aerogels collapse to a single curve simply by scaling in magnitude, matching the bulk I(T) data requires a 1.7°C shift of the bulk T_{NA} to lower temperatures (Fig. 4), as if the growth of B(T) in the aerogel is relative to a lower effective T_{NA}. This effect has not been calculated.
61. See note 10, (*13*).
62. η_B and η_K can be rigorously and accurately calculated for spatial dimension $D = 5 - \varepsilon$, when ε is small, but can only be roughly estimated for D = 3 (*24*, *26*).
63. L. Ricard, J. Prost, *J. Phys.* **40**, C-3 (1979).
64. ———, *J. Phys.* **42**, 861 (1981).
65. In aerogel, liquid crystals are transparent when isotropic but look like chalk when locally nematic or smectic, indicating that they scatter light entirely because of correlations in their optical anisotropy.
66. N. Menon, S. R. Nagle, *Phys. Rev. Lett.* **74**, 1230 (1995).
67. Whether this state, which is the one studied throughout this paper, has nematic disclinations or not, is a topic of current study. The wavelength dependence of the turbidity of nematics in aerosil indicates that they are present (*78*) and suggests that they are also present in the more strongly disordering aerogel. If they are absent, the state described here is the Nematic Elastic Glass (*26*, *68*, *69*).
68. See note 11, (*13*).
69. Because of the absence of topological defects and weak disorder, the description of the SmA Bragg glass is simple enough to enable analytical theory. This contrasts with fully topologically disordered glass states that do not have an obvious static order parameter and ultimately require a more subtle dynamical description, progress in which is only now beginning even for much simpler systems. Existence and properties of Bragg glasses have been recently actively investigated in the context of a vortex lattice in type II superconductors (*6*, *7*, *70*, *74*). The previously unknown SmA Bragg glass is the 3D smectic analog of the well-studied Cardy-Ostlund glass phase (*4*), which describes disordered vortex lines confined to a plane, and of the roughening of a crystal surface growing on a random substrate and other systems described by a 2D random-field XY-model (*5*).
70. T. Giamarchi, P. Le Doussal, *Phys. Rev. Lett.* **72**, 1530 (1994).
71. M. J. P. Gringas, D.A. Huse, *Phys. Rev. B* **53**, 15193 (1996).
72. D. S. Fisher, *Phys. Rev. Lett.* **78**, 1964 (1997).
73. L. Radzihovsky, *Bull. Am. Phys. Soc.* **43**, 193 (1998).
74. L. Balents, D. S. Fisher, L. Radzihovsky, private communication, unpublished theory.
75. $R(\tau) \sim \exp[-(\ln(\tau)/\ln(\tau_s))^2]$ is obtainable from a distribution of relaxation rates, which depend exponentially on a barrier height and are related to the size of the dynamical correlations (*76*, *77*).
76. D. S. Fisher, *Phys. Rev. Lett.* **56**, 416 (1986).
77. T. Ogielski, D. A. Huse, *Phys. Rev. Lett.* **56**, 1298 (1986).
78. T. Bellini *et al.*, *Phys. Rev. Lett.* **85**, 1008 (2000).
79. D. E. Feldman, *Phys. Rev. Lett.* **84**, 4886 (2000).
80. A. Maritan, M. Cieplak, T. Bellini, J. R. Banavar, *Phys. Rev. Lett.* **72**, 4113 (1994).

81. Supported by NSF Grants DMR 00-71989 and DMR 98-09555 (N.C.); INFM Paiss-C Grant (T.B.); NATO Collaborative Research Grant (T.B. and N.A.C.); David and Lucile Packard Foundation Fellowship, A. P. Sloan Foundation Fellowship, and NSF CAREER Grant DMR96-25111 (L.R.); NSF Grants DMR96-34596 and DMR99-80123 (J.T.). The authors are indebted to C. Garland for discussions. Research carried out in part at the National Synchrotron Light Source, Brookhaven National Laboratory, supported by DOE, Division of Materials Sciences and Division of Chemical Sciences.

15 November 2000; accepted 20 September 2001